The Astrophysical Journal, 701:1347–1356, 2009 August 20 doi:10.1088/0004-637X/701/2/1347

OPTICAL CONSTANTS OF AMORPHOUS AND CRYSTALLINE H_2O-ICE: 2.5–22 μm (4000–455 cm^{-1}) OPTICAL CONSTANTS OF H_2O-ICE

R. M. Mastrapa[1,2,4], S. A. Sandford[2], T. L. Roush[3], D. P. Cruikshank[2], and C. M. Dalle Ore[1,2]
[1] SETI Institute, 515 N. Whisman Road, Mountain View, CA 94043, USA; Rachel.M.Mastrapa@nasa.gov
[2] NASA Ames Research Center, MS 245-6, Moffett Field, CA 94035, USA
[3] NASA Ames Research Center, MS 245-3, Moffett Field, CA 94035, USA
Received 2009 April 14; accepted 2009 June 19; published 2009 July 31

ABSTRACT

Using new laboratory spectra, we have calculated the real and imaginary parts of the index of refraction of amorphous and crystalline H_2O-ice from 20–150 K in the wavelength range 2.5–22 μm (4000–455 cm^{-1}) and joined these results with previous measurement from 1.25 to 2.5 μm. These optical constants improve on previous measurements by having better temperature and spectral resolution and can be used to create model spectra for comparison to spectra of solar system objects and interstellar materials. In this wavelength range, the infrared band shapes and positions of amorphous H_2O-ice are strongly dependent on deposition temperature. Amorphous and crystalline H_2O-ice have distinctive spectral bands at all wavelengths in this region with bands weakening and shifting to shorter wavelength in amorphous H_2O-ice compared to crystalline H_2O-ice. Some notable exceptions are the band near 6 μm, which is stronger in amorphous H_2O-ice, and the bands near 4.5 μm and 12.5 μm, which shift to longer wavelength in amorphous H_2O-ice.

Key words: astrochemistry – infrared: solar system – interplanetary medium – methods: laboratory – planets and satellites: general

Online-only material: machine-readable table

1. INTRODUCTION

Although the presence of H_2O-ice on outer solar system objects has been known from infrared measurements for decades, there are still gaps in the lab measurements needed to further interpret the spectra of these bodies. The infrared absorption bands of H_2O-ice shift and change shape as a function of phase and temperature. However, the optical constants available for using in spectral models are at a limited range of temperatures and phases. The infrared range most useful for interpreting ground-based and spacecraft data of outer solar system bodies is ~1–5 μm, while data across the entire mid-infrared can assist with the interpretation of spectra of interstellar and protostellar ices. The range from 1.0 to 2.5 μm has been measured for amorphous and crystalline H_2O-ice at 10 K intervals over a broad temperature range (Grundy & Schmitt 1998; Mastrapa et al. 2008). Here we present measurements made in the mid-infrared, specifically 2.5–22 μm. We intend that these measurements support and improve analyses such as those by Hansen & McCord (2004), who examined this region in Galileo NIMS data to assess the distribution of amorphous and crystalline H_2O-ice on Ganymede.

The region near 3 μm of the H_2O-ice spectrum has been well studied (Bertie & Whalley 1964; Hale & Querry 1973; Whalley 1977; Bergren et al. 1978; Warren 1984; Warren & Brandt 2008) but usually at temperatures too high or too low for direct comparison to solar system objects. The optical constants of amorphous H_2O-ice are available at 10, 40, 80, 100, and 120 K (Hudgins et al. 1993), but these ices were all deposited at low temperature. In previous results (Mastrapa et al. 2008), the near-infrared bands of amorphous H_2O-ice look very different if they are deposited above or below 70 K, making it necessary to examine the changes in the mid-infrared bands with deposition temperature.

There is also a need for measurements of crystalline samples that are deposited at high temperature. Amorphous H_2O-ice samples heated to crystallization still contain a significant amount of amorphous H_2O-ice until heating to 180 K (Jenniskens et al. 1998). The near-infrared bands of H_2O-ice samples deposited at low temperature and heated to crystallization are weaker and shifted to shorter wavelength compared to samples deposited at 150 K (Mastrapa et al. 2008). The only available optical constants of crystalline H_2O-ice deposited at high temperature are only at 100 K (Bertie et al. 1969) and 163 K (Toon et al. 1994).

The main H_2O-ice bands and their assignments are given in Table 1. Since the absorptions of H_2O-ice are broad and their positions shift as a function of phase and temperature, we will assign general names to each major band to simplify the comparison of spectra of H_2O-ice at different temperatures or phases. The bands in this region include those near 6 μm (1667 cm^{-1}), near 4.5 μm (2200 cm^{-1}) and near 12 μm (830 cm^{-1}). The region between 2.5 and 3.5 μm contains the strongest absorption in this spectral range, which we will generally refer to as the 3 μm band. In crystalline H_2O-ice, this absorption feature consists of three separate bands: ~3.2 μm (3125 cm^{-1}), ~3.1 μm (3225 cm^{-1}), and ~3.0 μm (3333 cm^{-1}). In amorphous H_2O-ice there is one broad absorption near 3.1 μm (3225 cm^{-1}). The bands at ~3.0, 3.1, 3.2, and 6 μm are all molecular vibrations, the band near 12 μm is a lattice vibration, and the band near 4.5 μm is a combination mode of molecular and lattice vibrations.

2. MATERIALS AND METHODS

The vacuum system used in this work has remained unchanged since its last detailed description (Hudgins et al. 1993; Bernstein et al. 2006; Mastrapa et al. 2008). We collect infrared transmission spectra of ice samples under high vacuum

[4] Corresponding address: NASA Ames Research Center, Mail Stop 245-6, Moffett Field, CA 94035-1000, USA.

Table 1
Assignment of Bands for Amorphous and Crystalline H_2O-Ice

Crystalline[a]		Amorphous[b]		Assignment	A values [c]
cm^{-1}	μm	cm^{-1}	μm		(cm/molecule)
840	11.9	802	12.4	ν_R[d]	2.8×10^{-17}
1650	6.06	1660	6.02	ν_2[d]	1.0×10^{-17}
2266	4.41	2220	4.50	$\nu_2 + \nu_R$[d]	3.3×10^{-18}
3150	3.17	3191	3.13	ν_1 in-phase[e]	
3220	3.11	3253	3.07	ν_3 TO[e]	1.7×10^{-16}
3380	2.96	3367	2.97	ν_3 LO, ν_1 out-of-phase[e]	

Notes.
[a] From Bertie & Whalley (1964) at 100 K.
[b] From Hardin & Harvey (1973) at 92 K.
[c] From Hudgins et al. (1993).
[d] From Ockman (1958).
[e] From Whalley (1977).

(10^{-8} mbar) and low temperatures (15 K). The path of the infrared beam passes through the chamber windows and a KBr, ZnSe, or CsI sample window.

Our previous work included a detailed description of sample preparation and characterization (Mastrapa et al. 2008). We follow the same method in this work, the only difference being that the samples are significantly thinner. To create our samples, we first cooled the sample window to the desired temperature. We identify the phase of H_2O-ice, by the shape and position of the infrared bands in the context of the sample's temperature history. Although diffraction measurements are desirable, we do not have access to facilities with this capability. The amorphous samples were deposited at 15, 25, 40, 50, 60, 80, 100, and 120 K. All crystalline samples were deposited at 150 K because amorphous H_2O-ice can remain in the sample at high temperature (Jenniskens et al. 1998). There are variations in-band strength and position in the spectra of samples that are deposited at high temperature compared to those deposited at low temperature and annealed to the same temperature (Mastrapa et al. 2008). Once the sample window was cooled, we collected a background spectrum at a spectral resolution of 1 cm^{-1}, corresponding to a spectral resolution of 0.0002 μm at 1.1 μm, 0.0006 μm at 2.5 μm, and 0.05 μm at 22 μm.

To deposit samples, we injected purified (18.2 MΩ, freeze-pump-thawed to remove dissolved gases) H_2O–vapor into the vacuum chamber through a narrow inlet tube aimed at the sample window. During deposition, we directly measured the thickness of the samples by monitoring the interference fringes of a He–Ne laser reflected off the sample. The thickness of the ice was calculated using the equation:

$$d = (m\lambda_0)/(2n_{\rm ice}\cos\theta_{\rm ice}), \quad (1)$$

where m is the number of interference peaks, d is the ice thickness in μm, λ_0 is the wavelength of the laser (0.6328 μm), $n_{\rm ice}$ is the index of refraction of the ice at the laser wavelength (1.32 for crystalline H_2O-ice; Hale & Querry (1973), 1.29 for amorphous H_2O-ice; Westley et al. (1998); Dohnalek et al. (2003)), and $\theta_{\rm ice}$ is the angle of reflection within the ice sample. The creation of amorphous H_2O-ice samples requires a deposition rate of less than 0.01 g cm^{-2} hr (Beaumont et al. 1961). This corresponds to a deposition rate of 1.5 μm min^{-1} for I_ah (high-density amorphous H_2O-ice) and 2.0 μm min^{-1} for I_al (low-density amorphous H_2O-ice), using densities of 1.1 g cm^{-3} (Narten et al. 1976) and 0.82 g cm^{-3} (Westley et al. 1998), respectively. Both are larger than our average deposition rate of ~0.3 μm min^{-1}. For the 67 spectra used to calculate the optical constants, the sample thicknesses ranged between ~0.26 μm ($m = 0.5$) and ~0.36 μm ($m = 1.0$). The samples were sufficiently thick to display all of the relevant bands. The band near 3 μm is very strong and requires the creation of very thin samples to prevent saturation.

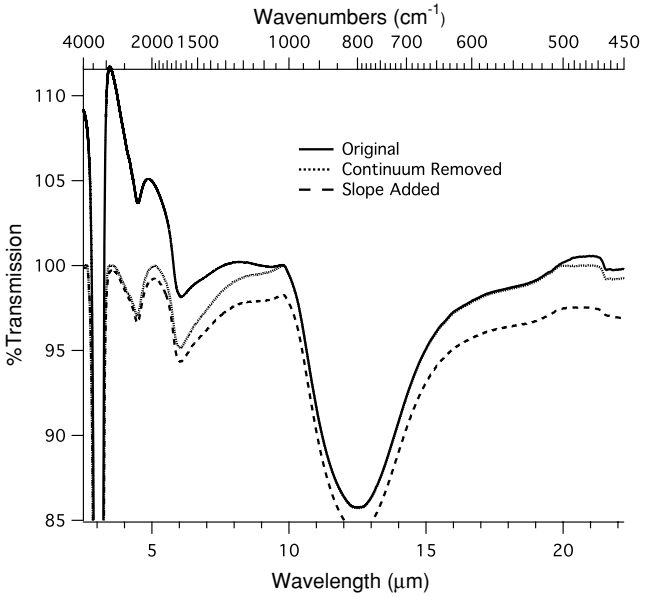

Figure 1. %Transmission spectra of amorphous H_2O-ice at 100 K, demonstrating the processing performed on the spectra. We remove the continuum from the original spectrum (black line) so that the transparent regions are close to 100% transmission (dotted line). We then adjust the slope of the spectrum to match previous work (dashed line).

Once the sample was deposited, we collected transmission spectra as the sample was warmed at 10 K intervals up to 120 K for amorphous H_2O-ice and 150 K for crystalline H_2O-ice. The temperature of the sample was increased at a rate of 1–2 K min^{-1} between measurements. The samples were left to stabilize for 5 minutes at each temperature, although we noted that any spectral changes occur within a minute of achieving the target temperature. Samples at the same temperature from different experiments were also compared to confirm the consistency of the spectral shapes. We collected measurements while heating as well as cooling to determine if the changes in band shapes were reversible. In general, the band changes were reversible within a given phase, i.e., the change between amorphous and crystalline H_2O-ice is irreversible, but the changes in band shape as a function of temperature in crystalline H_2O-ice is reversible.

Before calculating the optical constants, we removed the continuum from each spectrum (Figure 1). We removed the region near 4.26 μm in all spectra and the region from 15 to 20 μm in all crystalline spectra due to CO_2–gas contamination. We saw no temperature or phase dependence in the absolute value or slope of the continuum. We therefore subtracted the continuum from each spectrum to remove the effects of scattering. As noted previously (Mastrapa et al. 2008), we do not correct for surface reflection because the continuum correction is often an order of magnitude larger. The spectra were then adjusted to match the slope of Mukai & Krätschmer (1986) for the amorphous samples and Toon et al. (1994) for the crystalline samples. As noted previously (Mastrapa et al. 2008), the highest uncertainty in the measurements is restricted to the transparent regions of the spectrum. Small changes in continuum removal or slope can lead to large changes in absolute value in these regions.

Table 2.
Positions and Areas for the Band Near 12 μm (800 cm^{-1})

Phase	Temperature (K)	Left Bound		Right Bound		Position		A value (cm/molecule)
		cm^{-1}	μm	cm^{-1}	μm	cm^{-1}	μm	
I_c	20	1065	9.4	580	17.2	837	11.9	3.3×10^{-17}
I_c	30	1065	9.4	580	17.2	836	12.0	3.3×10^{-17}
I_c	40	1065	9.4	566	17.7	836	12.0	3.4×10^{-17}
I_c	50	1060	9.4	580	17.2	835	12.0	3.4×10^{-17}
I_c	60	1065	9.4	569	17.6	834	12.0	3.4×10^{-17}
I_c	70	1065	9.4	569	17.6	834	12.0	3.4×10^{-17}
I_c	80	1065	9.4	569	17.6	833	12.0	3.3×10^{-17}
I_c	90	1065	9.4	569	17.6	831	12.0	3.3×10^{-17}
I_c	100	1062	9.4	576	17.4	830	12.1	3.2×10^{-17}
I_c	110	1065	9.4	569	17.6	828	12.1	3.1×10^{-17}
I_c	120	1065	9.4	569	17.6	828	12.1	3.1×10^{-17}
I_c	130	1065	9.4	566	17.7	828	12.1	3.0×10^{-17}
I_c	140	1065	9.4	566	17.7	826	12.1	2.9×10^{-17}
I_c	150	1062	9.4	548	18.2	825	12.1	3.0×10^{-17}
I_a	15	1037	9.6	503	19.9	754	13.3	2.5×10^{-17}
I_a	25	1022	9.8	469	21.3	763	13.1	2.5×10^{-17}
I_a	40	1020	9.8	503	19.9	769	13.0	2.3×10^{-17}
I_a	50	1014	9.9	483	20.7	779	12.8	2.6×10^{-17}
I_a	60	1020	9.8	505	19.8	783	12.8	2.3×10^{-17}
I_a	80	1020	9.8	501	19.9	795	12.6	3.0×10^{-17}
I_a	100	1019	9.8	532	18.8	800	12.5	3.0×10^{-17}
I_a	120	1020	9.8	525	19.0	805	12.4	3.2×10^{-17}

3. SPECTRAL ANALYSIS

3.1. Calculation of n and k

We follow the procedure for calculating optical constants described previously (Bergren et al. 1978; Heavens 1991; Hudgins et al. 1993; Mastrapa et al. 2008). However, to avoid infrared fringes in the model spectrum, we use an approximation for thick samples to calculate α and k from the measured spectra:

$$\alpha \equiv 4\pi k\nu = \frac{1}{d}\ln\left(\frac{I_0}{I}\right), \quad (2)$$

where d is the thickness of the ice and I/I_0 is the transmission spectrum of the ice. Once we calculated α, we averaged together α-spectra of samples of the same phase and the same temperature, but different thicknesses. These α-spectra ranging from 2.5 to 20 μm were then joined to previous measurements that covered the range from 1.25 to 2.5 μm (Mastrapa et al. 2008). We then used α to derive n as a function of wavenumber (ν) via the Kramers–Kronig relationship:

$$n(\nu) = n_1^0 + \frac{1}{2\pi^2}\int_0^\infty \frac{\alpha(\nu')}{\nu'^2 - \nu^2}\,d\nu', \quad (3)$$

where n_1^0 is a seed value for the real part of the index of refraction (1.32 for crystalline H_2O-ice; Hale & Querry 1973, 1.29 for amorphous H_2O-ice; Westley et al. 1998). In this way, n starts as a constant as a function of wavelength, but is recalculated to be a function of wavelength depending on the value of α.

3.2. Calculation of A Values

We calculated the intrinsic strength of absorption features in cm/molecule, or A values, following the method of Hudgins et al. (1993). As with their work, we needed to multiply the integrated areas of our bands by 2.303 to convert from a base 10 logarithm to natural logarithm. The A value is given by

$$A = N^{-1}\int \tau\,d\nu, \quad (4)$$

where N is the column density of the sample (number of absorbers per cm^2) ν is in wavenumbers, and τ is

$$\tau \equiv \ln(I_0/I), \quad (5)$$

where I is the intensity of light with the sample, and I_0 is the intensity of light without the sample. The column density of the sample was calculated by multiplying the thickness and density of the sample by Avogadro's number, and then dividing by the molecular weight of the material. The densities used are as follows: I_ah – 1.1 g cm^{-3} (Narten et al. 1976), I_al – 0.82 g cm^{-3} (Westley et al. 1998), and I_c – 0.931 g cm^{-3} (78 K) (Petrenko & Whitworth 1999). We calculated A values for all bands (Tables 2–7). Since the H_2O-ice bands are broad and the limits are difficult to determine, we include the boundary values over which areas are integrated.

4. RESULTS

4.1. Amorphous H_2O-Ice

The general shapes of our amorphous spectra are in agreement with previous measurements (Mukai & Krätschmer 1986; Hudgins et al. 1993; Figure 2). We also include optical constants in this range for crystalline H_2O-ice at 266 K (Warren & Brandt 2008). These measurements of comparatively warm H_2O-ice are more similar in shape to our amorphous measurements than to our crystalline spectra. However, there are still significant differences, especially near 3 μm. Compared to this work, the bands in Hudgins et al. are slightly narrower, weaker, and shifted to a shorter wavelength. The location of the 3 μm feature is shifted to slightly longer wavelength in the spectrum

Table 3.
Positions and Areas for the Band Near 6 μm (1667 cm^{-1})

Phase	Temperature (K)	Left Bound		Right Bound		Position		A value (cm/molecule)
		cm^{-1}	μm	cm^{-1}	μm	cm^{-1}	μm	
I_c	20	1997	5.0	1085	9.2	1564	6.4	2.0×10^{-17}
I_c	30	2005	5.0	1085	9.2	1564	6.4	2.0×10^{-17}
I_c	40	2008	5.0	1083	9.2	1557	6.4	1.9×10^{-17}
I_c	50	2002	5.0	1078	9.3	1560	6.4	1.9×10^{-17}
I_c	60	2007	5.0	1083	9.2	1567	6.4	1.9×10^{-17}
I_c	70	2007	5.0	1082	9.2	1571	6.4	1.9×10^{-17}
I_c	80	2004	5.0	1079	9.3	1574	6.4	1.9×10^{-17}
I_c	90	1998	5.0	1077	9.3	1579	6.3	1.8×10^{-17}
I_c	100	1996	5.0	1075	9.3	1570	6.4	1.8×10^{-17}
I_c	110	1993	5.0	1069	9.4	1582	6.3	1.8×10^{-17}
I_c	120	1993	5.0	1069	9.4	1599	6.3	1.8×10^{-17}
I_c	130	1998	5.0	1068	9.4	1615	6.2	1.7×10^{-17}
I_c	140	1988	5.0	1060	9.4	1619	6.2	1.7×10^{-17}
I_c	150	1988	5.0	1061	9.4	1624	6.2	1.7×10^{-17}
I_a	15	1953	5.1	1065	9.4	1668	6.0	1.1×10^{-17}
I_a	25	1929	5.2	1018	9.8	1666	6.0	9.5×10^{-18}
I_a	40	1927	5.2	1045	9.6	1671	6.0	1.1×10^{-17}
I_a	50	1936	5.2	1028	9.7	1672	6.0	1.2×10^{-17}
I_a	60	1924	5.2	1040	9.6	1672	6.0	1.1×10^{-17}
I_a	80	1927	5.2	1038	9.6	1663	6.0	1.5×10^{-17}
I_a	100	1927	5.2	1032	9.7	1655	6.0	1.6×10^{-17}
I_a	120	1915	5.2	1025	9.8	1655	6.0	1.7×10^{-17}

Table 4.
Positions and Areas for the Band Near 4.5 μm (2222 cm^{-1})

Phase	Temperature (K)	Left Bound		Right Bound		Position		A value (cm/molecule)
		cm^{-1}	μm	cm^{-1}	μm	cm^{-1}	μm	
I_c	20	2935	3.4	2005	5.0	2268	4.4	1.3×10^{-17}
I_c	30	2935	3.4	2005	5.0	2268	4.4	1.3×10^{-17}
I_c	40	2898	3.5	2005	5.0	2268	4.4	1.2×10^{-17}
I_c	50	2840	3.5	1999	5.0	2264	4.4	1.2×10^{-17}
I_c	60	2881	3.5	2005	5.0	2264	4.4	1.2×10^{-17}
I_c	70	2881	3.5	2005	5.0	2264	4.4	1.2×10^{-17}
I_c	80	2866	3.5	2002	5.0	2264	4.4	1.1×10^{-17}
I_c	90	2857	3.5	1997	5.0	2263	4.4	1.1×10^{-17}
I_c	100	2819	3.5	1995	5.0	2259	4.4	1.1×10^{-17}
I_c	110	2845	3.5	1997	5.0	2261	4.4	1.1×10^{-17}
I_c	120	2819	3.5	1997	5.0	2259	4.4	1.0×10^{-17}
I_c	130	2815	3.6	2001	5.0	2255	4.4	9.9×10^{-18}
I_c	140	2796	3.6	1986	5.0	2255	4.4	9.8×10^{-18}
I_c	150	2772	3.6	1997	5.0	2252	4.4	9.7×10^{-18}
I_a	15	2795	3.6	1957	5.1	2213	4.5	4.9×10^{-18}
I_a	25	2737	3.7	1957	5.1	2209	4.5	4.3×10^{-18}
I_a	40	2855	3.5	1943	5.1	2225	4.5	6.0×10^{-18}
I_a	50	2758	3.6	1947	5.1	2225	4.5	5.6×10^{-18}
I_a	60	2864	3.5	1951	5.1	2231	4.5	6.5×10^{-18}
I_a	80	2862	3.5	1948	5.1	2237	4.5	9.3×10^{-18}
I_a	100	2829	3.5	1949	5.1	2239	4.5	9.8×10^{-18}
I_a	120	2890	3.5	1935	5.2	2241	4.5	9.7×10^{-18}

from Mukai & Krätschmer. Overall, the present work represents the improvement in spectral resolution compared to Mukai & Krätschmer, and a smoother transition between strong features and transparent regions when compared to Hudgins et al.

These differences in strength and band position could be due to differences in laboratory methods, but may also represent the strong temperature variability in amorphous H_2O-ice. Note that the transparent region near 3.5 μm is shifted to longer wavelengths in both previous measurements compared to this work. This is most likely a result of the aforementioned uncertainty in removing the continuum, and should not be over-interpreted.

In our work, the shape of the 3 μm band is strongly dependent on the deposition temperature: it grows stronger and shifts to longer wavelength as deposition occurs at higher temperatures (Figure 3). Unlike in previous measurements where there was a clear grouping of band shapes above and below 70 K (Mastrapa et al. 2008), there is a broad range of changes as a function

Table 5.
Positions and Areas for the Band Near 3.1 μm (3226 cm^{-1})

Phase	Temperature (K)	Left Bound		Right Bound		Position		A value (cm/molecule)
		cm^{-1}	μm	cm^{-1}	μm	cm^{-1}	μm	
I_c	20	4695	2.13	2980	3.36	3210	3.12	3.0×10^{-16}
I_c	30	4695	2.13	2980	3.36	3210	3.12	3.0×10^{-16}
I_c	40	4695	2.13	2980	3.36	3210	3.11	3.0×10^{-16}
I_c	50	4695	2.13	2980	3.36	3211	3.11	2.9×10^{-16}
I_c	60	4695	2.13	2980	3.36	3212	3.11	2.9×10^{-16}
I_c	70	4695	2.13	2931	3.41	3213	3.11	2.9×10^{-16}
I_c	80	4695	2.13	2931	3.41	3214	3.11	2.9×10^{-16}
I_c	90	4695	2.13	2931	3.41	3215	3.11	2.8×10^{-16}
I_c	100	4605	2.17	2931	3.41	3216	3.11	2.8×10^{-16}
I_c	110	4605	2.17	2931	3.41	3218	3.11	2.7×10^{-16}
I_c	120	4605	2.17	2890	3.46	3219	3.11	2.7×10^{-16}
I_c	130	4575	2.19	2860	3.50	3220	3.11	2.7×10^{-16}
I_c	140	4575	2.19	2860	3.50	3222	3.10	2.7×10^{-16}
I_c	150	4384	2.28	2853	3.51	3224	3.10	2.7×10^{-16}
I_a	15	4320	2.31	2933	3.41	3298	3.03	1.9×10^{-16}
I_a	25	3825	2.61	2727	3.67	3280	3.05	1.9×10^{-16}
I_a	40	4320	2.31	2957	3.38	3279	3.05	2.1×10^{-16}
I_a	50	3990	2.51	2798	3.57	3265	3.06	2.1×10^{-16}
I_a	60	4320	2.31	2961	3.38	3264	3.06	2.1×10^{-16}
I_a	80	4320	2.31	2956	3.38	3257	3.07	2.9×10^{-16}
I_a	100	4249	2.35	2905	3.44	3254	3.07	3.0×10^{-16}
I_a	120	4320	2.31	2958	3.38	3252	3.08	3.0×10^{-16}

Table 6.
Positions and Areas for the Band Near 3.2 μm (3125 cm^{-1})

Phase	Temperature (K)	Left Bound		Right Bound		Position		A value (cm/molecule)
		cm^{-1}	μm	cm^{-1}	μm	cm^{-1}	μm	
I_c	20	3170	3.15	3070	3.26	3129	3.20	2.0×10^{-17}
I_c	30	3170	3.15	3070	3.26	3129	3.20	2.0×10^{-17}
I_c	40	3170	3.15	3070	3.26	3131	3.19	1.9×10^{-17}
I_c	50	3170	3.15	3070	3.26	3130	3.20	1.8×10^{-17}
I_c	60	3171	3.15	3070	3.26	3131	3.19	1.8×10^{-17}
I_c	70	3172	3.15	3071	3.26	3134	3.19	1.6×10^{-17}
I_c	80	3175	3.15	3074	3.25	3137	3.19	1.6×10^{-17}
I_c	90	3175	3.15	3075	3.25	3136	3.19	1.4×10^{-17}
I_c	100	3175	3.15	3078	3.25	3138	3.19	1.3×10^{-17}
I_c	110	3176	3.15	3079	3.25	3141	3.18	1.2×10^{-17}
I_c	120	3182	3.14	3079	3.25	3142	3.18	1.1×10^{-17}
I_c	130	3186	3.14	3083	3.24	3146	3.18	1.0×10^{-17}
I_c	140	3186	3.14	3083	3.24	3146	3.18	9.2×10^{-18}
I_c	150	3189	3.14	3089	3.24	3140	3.18	8.2×10^{-18}

Table 7.
Positions and Areas for the Band Near 3 μm (3333 cm^{-1})

Phase	Temperature (K)	Left Bound		Right Bound		Position		A value (cm/molecule)
		cm^{-1}	μm	cm^{-1}	μm	cm^{-1}	μm	
I_c	20	3435	2.91	3310	3.02	3371	2.97	4.3×10^{-18}
I_c	30	3435	2.91	3310	3.02	3371	2.97	4.3×10^{-18}
I_c	40	3439	2.91	3311	3.02	3372	2.97	4.4×10^{-18}
I_c	50	3438	2.91	3311	3.02	3372	2.97	4.2×10^{-18}
I_c	60	3438	2.91	3311	3.02	3373	2.96	4.1×10^{-18}
I_c	70	3438	2.91	3311	3.02	3374	2.96	3.9×10^{-18}
I_c	80	3447	2.90	3314	3.02	3375	2.96	3.9×10^{-18}
I_c	90	3447	2.90	3314	3.02	3376	2.96	3.7×10^{-18}
I_c	100	3447	2.90	3314	3.02	3378	2.96	3.5×10^{-18}
I_c	110	3447	2.90	3314	3.02	3379	2.96	3.4×10^{-18}
I_c	120	3447	2.90	3314	3.02	3380	2.96	3.2×10^{-18}
I_c	130	3453	2.90	3316	3.02	3382	2.96	3.1×10^{-18}
I_c	140	3453	2.90	3320	3.01	3383	2.96	2.9×10^{-18}
I_c	150	3452	2.90	3320	3.01	3385	2.95	2.9×10^{-18}

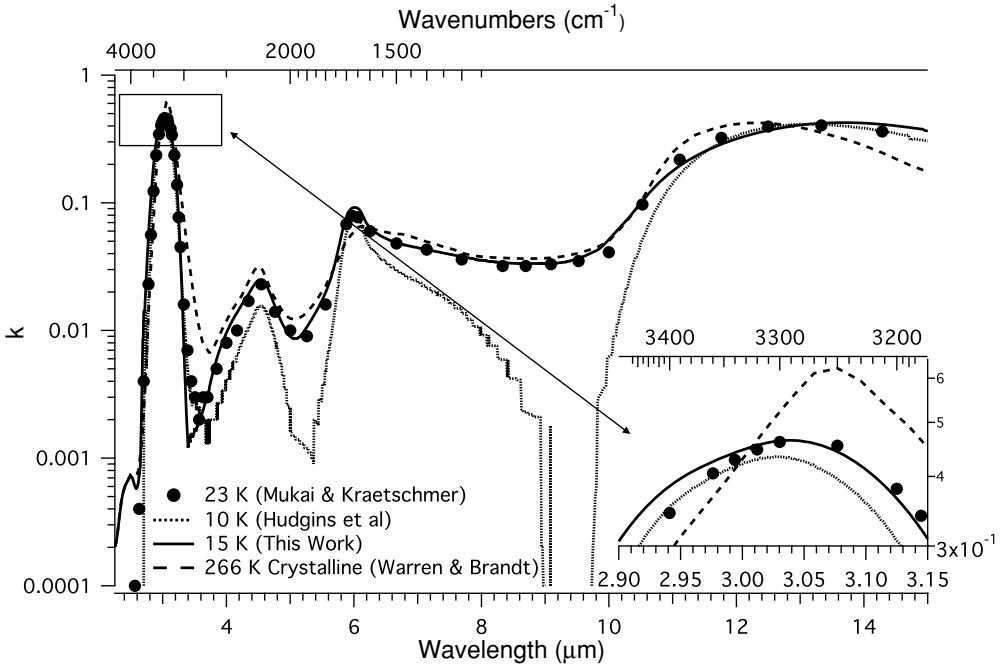

Figure 2. *k* spectra of amorphous H_2O-ice from this work (solid line) deposited at 15 K (solid line) compared to those of Mukai and Krätschmer (1986) at 23 K, Hudgins et al. (1993) at 10 K (dotted line), and Warren and Brandt (2008) at 266 K (dashed line).

of deposition temperature. Temperature cycling of the samples demonstrated that the changes in band shape are irreversible, that is, a sample deposited at 15 K, heated to 100 K, and cooled back to 15 K retains the band shape seen at 100 K.

The rest of the spectral bands also change shape with deposition temperature, but the changes are not as large as the changes seen in the 3 μm band. However, there are two significant differences: the band near 6 μm is stronger at low temperature, and the band near 12 μm shifts to shorter wavelength with increasing temperature. These changes are also irreversible.

4.2. Crystalline H_2O-Ice

Although it has long been assumed that there are no spectral differences between I_h and I_c (Bertie & Whalley 1964), there may be differences in the band shapes (Hardin & Harvey 1973; Mastrapa et al. 2008). We compare our crystalline H_2O-ice spectra with measurements of I_h (hexagonal H_2O-ice) at 163 K (Toon et al. 1994) and 100 K (Bertie et al. 1969; Figure 4). Ideally, we would compare our results to the constants from Curtis et al. (2005). However, the region that overlaps with their results, 15–20 μm, was trimmed from our crystalline spectra due to contamination. The overall shapes of the bands are similar among all measurements, but there are some differences in band position and strength. In previous measurements (Bertie et al. 1969; Toon et al. 1994), there is no clear difference between measurements at 100 K and at 163 K. However, the 3 μm band in our measurements of crystalline H_2O-ice at 100 K is stronger and shifted to longer wavelength compared to other spectra. Since our samples are likely to be I_c, this is another example of the difference between I_c and I_h.

Our work has higher spectral resolution than that of earlier studies, making it possible to clearly delineate the side feature near 3100 cm^{-1} (3.2 μm). Previous measurements included only a few data points in that region, making it impossible to capture the variation in the *n* values. There is a difference in the location

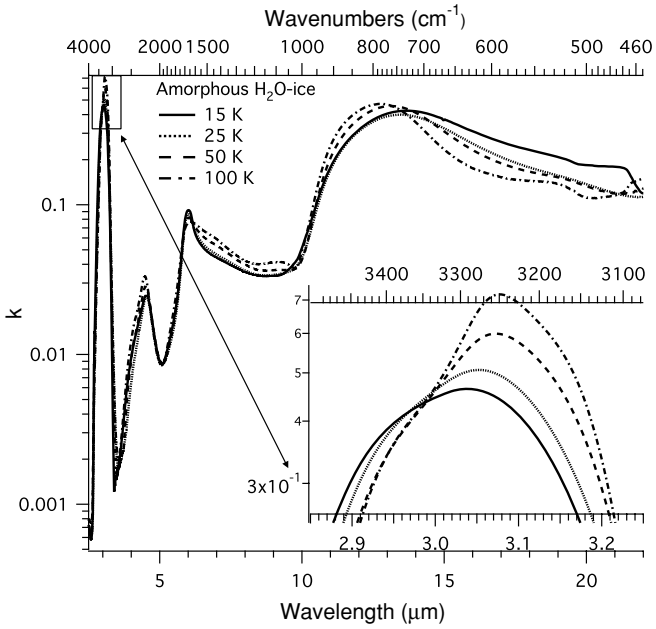

Figure 3. *k* spectra of amorphous H_2O-ice deposited at a range of temperatures: 15 K (solid line), 25 K (dotted line), 50 K (dashed line), and 100 K (dot-dash line).

of the transparent region near 3.5 μm, similar to that seen in the amorphous spectra. This could be a result of differences in the ice samples, but it is more likely a product of continuum removal.

Both the band near 3.1 μm and the band near 3.2 μm are temperature dependent, (Figure 5). Both bands grow stronger and shift to longer wavelength with decreasing temperature. The band near 3.2 μm changes from a small shoulder at 150 K, to a prominent feature at 20 K. This behavior is the same for all features, except for the 12 μm libration band, which shifts to longer wavelength with increasing temperature.

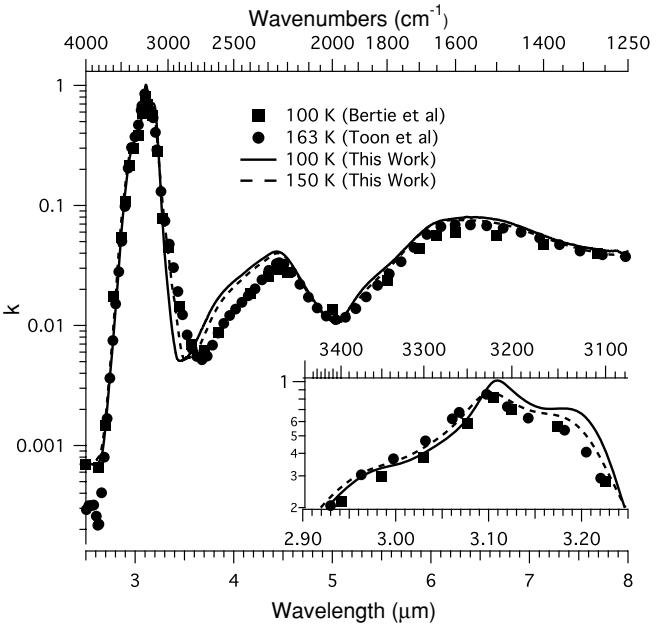

Figure 4. *k* spectra of crystalline H_2O-ice from this work at 100 K (solid line) and 150 K (dashed line). Also included are *k* spectra of I_h at 163 K from Toon et al. (1994) and at 100 K from Bertie et al. (1969).

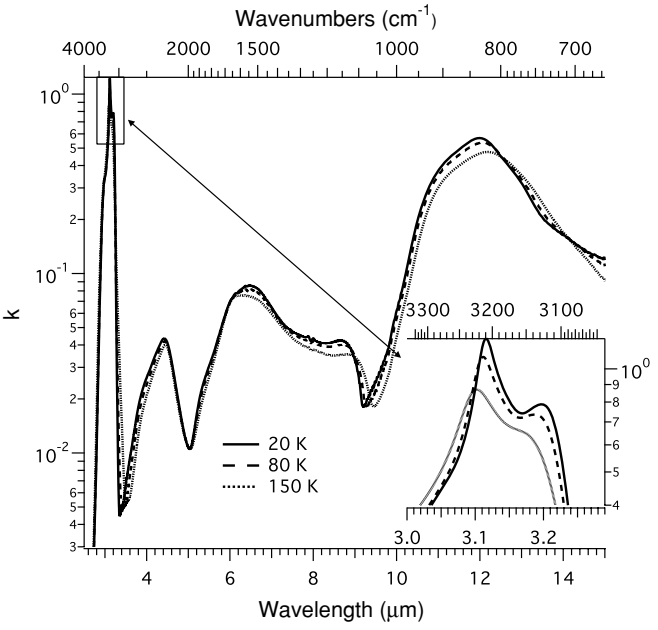

Figure 5. *k* spectra of crystalline H_2O-ice at 20 K (solid line), 80 K (dashed line), and 150 K (dotted line).

4.3. Comparing Phases

We compare the spectra of amorphous and crystalline H_2O-ice to demonstrate the distinguishing features between the phases (Figure 6). The band near 3 μm is stronger and shifted to longer wavelength in crystalline H_2O-ice compared to that of amorphous H_2O-ice. This is due to the increased hydrogen bonding in the crystalline ice. This feature consists of one central component and two shoulders in the crystalline sample, while the amorphous sample shows a single broad feature. At 120 K the amorphous 3 μm band is sharper, but still does not display the triple structure seen in crystalline H_2O-ice.

The combination band near 4.5 μm has a similar shape for both phases over the temperature range 15–120 K (Figure 6). The transparent regions next to the band are offset from one another as a function of H_2O-ice phase. Since, the transparent regions near 3.5 μm and 5.0 μm have a higher level of uncertainty in their absolute value and because the overall slope of the spectrum was set to match previous work, these offsets in the transparent regions should not be interpreted as actual phase-dependent changes in the spectrum. Future measurements will be needed to minimize the uncertainty in these regions for them to be properly interpreted.

Hagen & Tielens (1982) demonstrated that the 6 μm band is sharper and stronger in amorphous than in crystalline H_2O-ice, as we also find (Figure 7). This band seems to be the only exception to the phase-dependent behavior of the infrared bands of H_2O-ice since they generally are weaker and broader in amorphous compared to crystalline H_2O-ice (Schmitt et al. 1998; Mastrapa et al. 2008). Our results agree with the earlier work, although we show that the difference is not as large at high temperature. At 120 K, the 6 μm band is similar in strength in amorphous and crystalline H_2O-ice, although the amorphous band is still narrower.

The 12 μm band shifts in the opposite direction when compared to the 3 μm and 6 μm bands. The amorphous 12 μm band shifts to longer wavelength compared to the crystalline band. In the next section, we quantify these qualitative changes in band position.

4.4. Band Locations and A Values

The locations of all bands are given in Tables 2–7. To quantify the changes in band location with phase and temperature, we subtracted the value at 20 K in crystalline H_2O-ice from the location of each band (Figure 8). The bands near 2.9 μm and 3.2 μm were omitted because they are not strongly temperature dependent and they mirror the behavior of the band near 3.1 μm.

Some of the bands show a large shift in position as a function of temperature. For example, the amorphous band near 12 μm shifts almost a full μm between 20 and 120 K. The next largest shifts due to temperature are shown by the crystalline bands near 6 and 12 μm which both shift ~0.2 μm between 20 and 150 K. The rest of the bands demonstrate shifts of 0.1 μm or less over the full range of temperatures. The smallest temperature-based shift is seen in the crystalline 3.1 μm band, which only shifts ~0.01 μm between 20 and 150 K, making this band an unlikely candidate for determining remote temperature estimates by spectroscopy.

All bands shift as a function of phase. The amorphous bands near 6 and 12 μm have the largest shifts from the crystalline bands. The amorphous 12 μm band shifts from a minimum of 0.4 μm at 120 K to a maximum of 1.4 μm at 20 K from the crystalline band. The amorphous 6 μm band is shifted a minimum of 0.2 and a maximum of 0.4 μm from the crystalline values. The remaining two amorphous bands are much closer to the crystalline bands: they are shifted ~0.1 μm at 20 K and ~0.04 μm at 120 K.

For each band, the sign of the shift is dependent on phase, as demonstrated by Hardin & Harvey (1973). The crystalline 3 μm and 6 μm bands shift to shorter wavelength with increasing temperature, while the same bands in amorphous H_2O-ice shift to longer wavelength with increasing temperature. As the temperature increases, the 4.5 μm and 12 μm bands shift to longer wavelength in crystalline H_2O-ice and shorter wavelength in amorphous H_2O-ice.

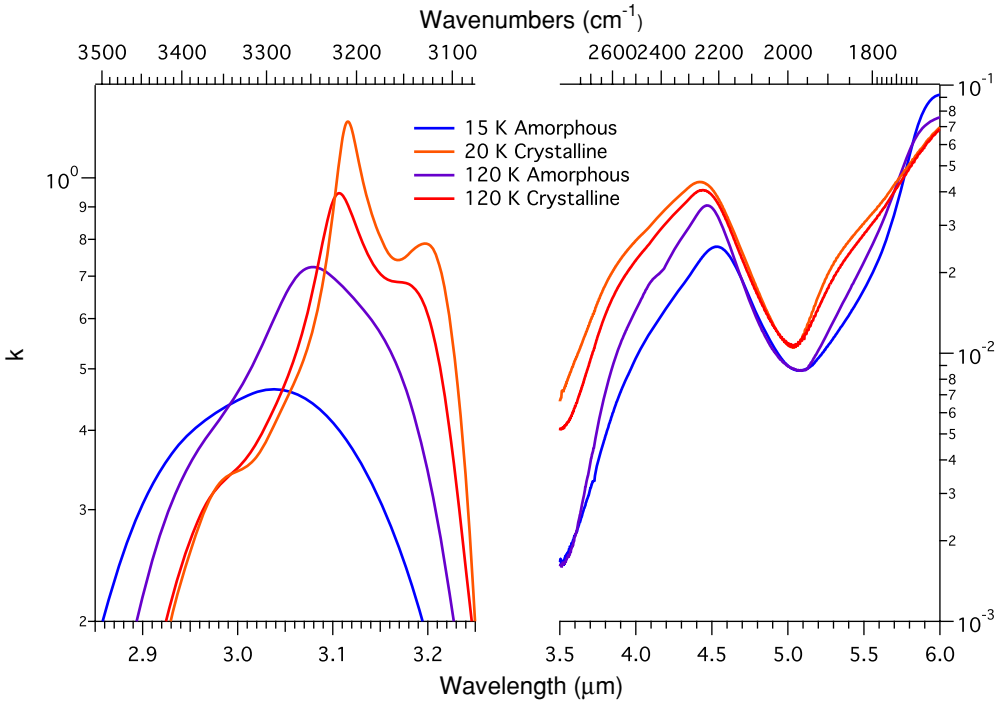

Figure 6. *k* spectra of amorphous and crystalline H_2O-ice. Crystalline spectra are at 20 K (orange line) and 120 K (purple line). Amorphous spectra are at 15 K (blue line) and 120 K (purple line).

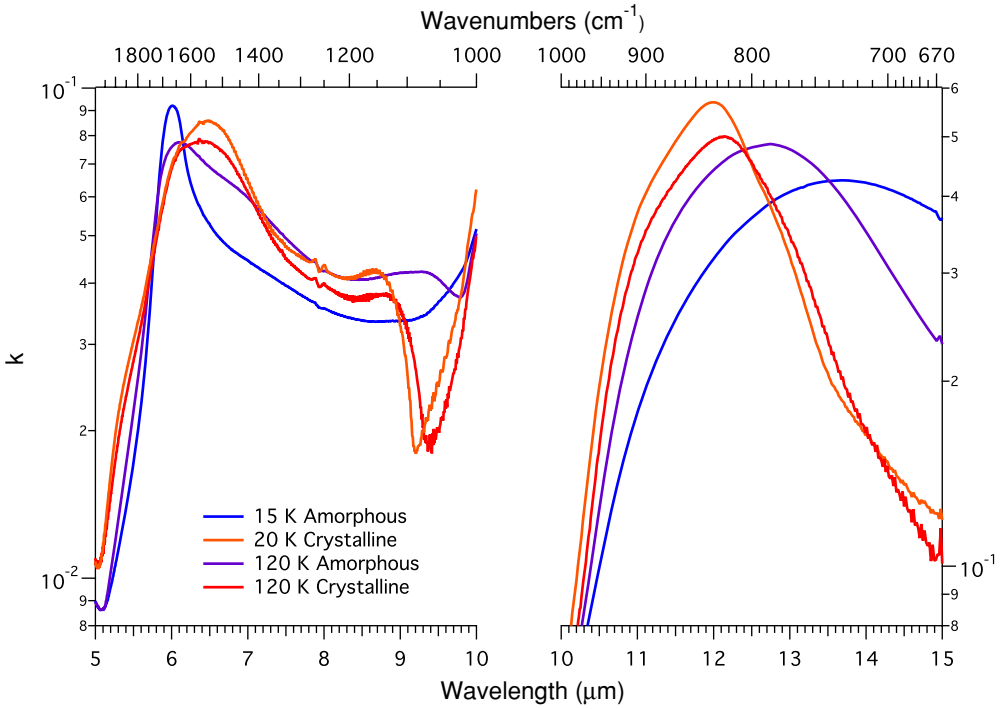

Figure 7. *k* spectra of amorphous and crystalline H_2O-ice. Crystalline spectra are at 20 K (orange line) and 120 K (purple line). Amorphous spectra are at 15 K (blue line) and 120 K (purple line).

As seen above, the bands can be split into two groups based on which direction they shift as a function of temperature. These two groups also shift in the same direction based on phase. For example, the 3 μm and 6 μm bands are both shifted to shorter wavelength relative to the amorphous bands, while the shift is opposite for the 4.5 μm and 12 μm bands. The shifting of these bands appears to be dependent on the type of vibration since the 3 μm and 6 μm bands are molecular vibrations, while the 4.5 μm and 12 μm bands are (at least in part) lattice vibrations (Table 1).

The *A* values of the bands also change as a function of temperature and phase (Figure 9). The *A* values for the crystalline bands are larger than their amorphous counterparts at low temperature. Near 80 K, the *A* values are indistinguishable between the phases. Also, all of the crystalline *A* values grow smaller with increasing temperature. As with the shifts in band

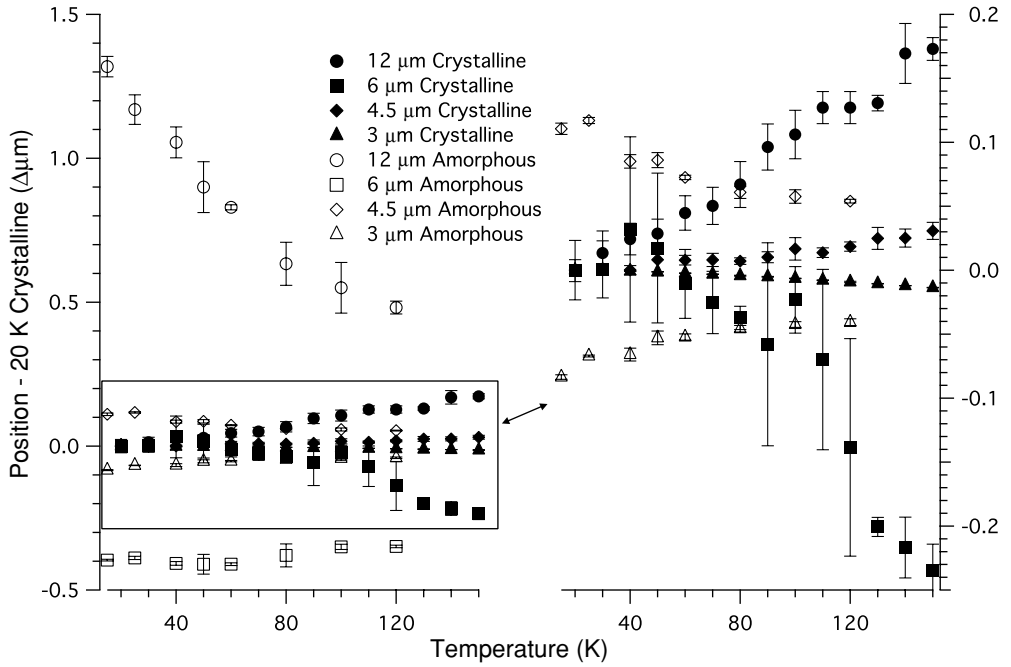

Figure 8. Positions of the bands of amorphous and crystalline H_2O-ice relative to the value of the crystalline band at 20 K: 12 μm (circles), 6 μm (squares), 4.5 μm (diamonds), and 3 μm (triangles). All crystalline bands have filled symbols while all amorphous bands have empty symbols.

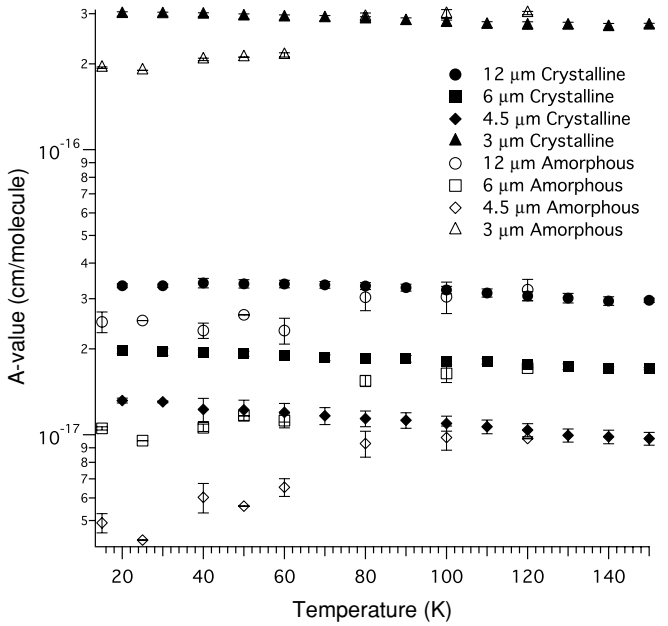

Figure 9. *A* values of the bands of amorphous and crystalline H_2O-ice.

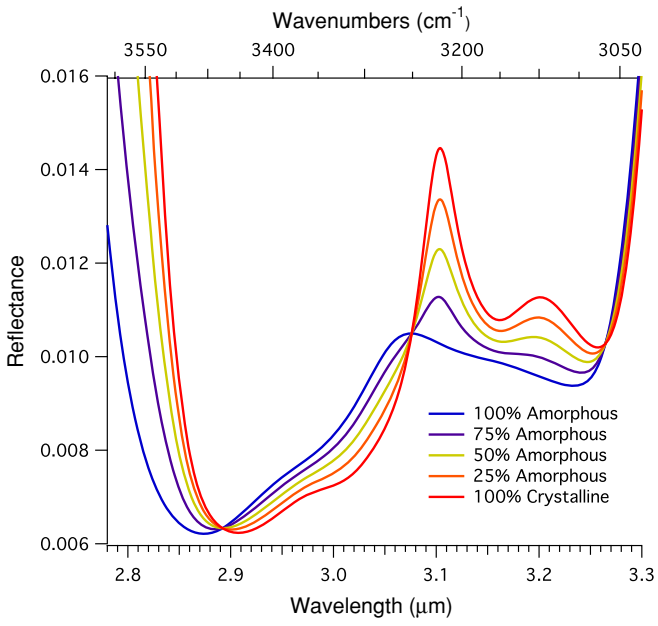

Figure 10. Model mixtures of amorphous and crystalline H_2O-ice at 100 K, with grain sizes of 20 μm. Mixtures ratios include: 100% amorphous (blue), 75% amorphous (purple), 50% amorphous (tan), 25% amorphous (orange), and 100% crystalline (red).

position, the changes in *A* value are reversible as long as the sample does not change phase. The amorphous samples that are heated maintain their larger *A* values when cooled, while the *A* values of the crystalline samples are reversible.

4.5. Reflectance Models

The measurements presented in this paper have been joined with our previous work (Mastrapa et al. 2008) to create a set of optical constants from 1.25 to 22 μm for H_2O-ice. These constants can be used to create model reflectance, transmission, and scattering spectra. For example, an early version of our results was used to model reflectance spectra of Quaoar (Dalle Ore et al. 2009).

We have calculated reflectance spectra of several mixtures of amorphous and crystalline H_2O-ice at 100 K following the method described in Roush (1994; Figure 10). Although interstellar objects are easily observed in the region near 3 μm, the 3 μm band is difficult to observe on solar system objects from ground-based telescopes. However, this region is easily measured by spacecraft instruments such as Galileo NIMS and Cassini VIMS. Hansen & McCord (2004) examined this region in NIMS data to assess the distribution of amorphous and crystalline H_2O-ice on Ganymede.

Table 8
Optical Constant of Amorphous H_2O-ice at 15 K

Wavelength (μm)	n	k
1.1111962	1.2835379	2.4214661e-06
1.1113154	1.2835368	4.2869903e-06
1.1114346	1.2835363	5.5180968e-06
1.1115538	1.2835360	5.7439300e-06
1.1116730	1.2835354	5.3265765e-06

(This table is available in its entirety in a machine-readable form in the online journal. A portion is shown here for guidance regarding its form and content.)

The main region of interest is near 3 μm. All model spectra demonstrate the Fresnel peak, but the pure crystalline spectrum has two peaks while the pure amorphous spectrum has one. The position of the peaks is controlled by the pure crystalline spectrum. The strongest peak near 3.1 μm does not shift from the pure crystalline position even when the content is 75% amorphous. The band near 3.2 μm gets steadily weaker with increasing amorphous content until it disappears completely. The band near 4.5 μm does not show a strong dependence on amorphous content.

5. CONCLUSIONS

We present optical constants of crystalline and amorphous H_2O-ice from 2.5 to 22 μm and draw the following conclusions from our measurements. All bands change position and shape as a function of phase and temperature. The largest changes in position as a function of temperature and phase are seen in the 6 μm and 12 μm bands. The optical constants for these bands may be useful for the interpretation of spectra of interstellar and protostellar objects, and may also be used for thermal emission spectra of solar system objects from spacecraft measurements. Of all the bands studied, the 4.5 μm band is the least useful for remotely assessing phase or temperature because the changes in position are small compared to the other bands. The 3 μm band has been used to remotely determine the phase of interstellar H_2O-ice, and can also be used to analyze spacecraft measurements of solar system objects.

Regarding the application of these constants, we would recommend attempting to match the appropriate temperature spectrum to the estimated temperature of the object. Although these measurements are from thin, vapor-deposited samples, the optical constants can be applied to transmission or reflectance observations using the appropriate models. As for the phase of H_2O-ice, the presence of amorphous H_2O-ice should be obvious from shifts in the infrared bands. Our crystalline spectra are assumed to be I_c, a meta-stable phase of H_2O-ice. It is unclear whether this phase would be present on icy solar system objects or if it would fully convert to I_h. However, the spectral difference between I_h and I_c are subtle compared to using H_2O-ice spectra at the wrong temperature. Until further I_h measurements can be made, I_c is a reasonable substitute.

All optical constants are available online, and Table 8 shows an example.

R.M.M., S.A.S., and T.L.R. acknowledge support via NASA's Planetary Geology and Geophysics Program, Proposal 05-PGG05-41.

REFERENCES

Beaumont, R. H., Chihara, H., & Morrison, J. A. 1961, J. Chem. Phys., 34, 1456
Bergren, M. S., Schuh, D., Sceats, M. G., & Rice, S. A. 1978, J. Chem. Phys., 69, 3477
Bernstein, M. P., Cruikshank, D. P., & Sandford, S. A. 2006, Icarus, 181, 302
Bertie, J. E., Labbe, H. J., & Whalley, E. 1969, J. Chem. Phys., 50, 4501
Bertie, J. E., & Whalley, E. 1964, J. Chem. Phys., 40, 1637
Curtis, D. B., Rajaram, B., Toon, O. B., & Tolbert, M. A. 2005, Appl. Opt., 44, 4102
Dalle Ore, C. M., et al. 2009, A&A, in press
Dohnalek, Z., Kimmel, G. A., Ayotte, P., Smith, R. S., & Kay, B. D. 2003, J. Chem. Phys., 118, 364
Grundy, W. M., & Schmitt, B. 1998, J. Geophys. Res., 103, 25809
Hagen, W., & Tielens, A. G. G. M. 1982, Spectochim. Acta, 38A, 1089
Hale, G. M., & Querry, M. R. 1973, Appl. Opt., 12, 555
Hansen, G. B., & McCord, T. B. 2004, J. Geophys. Res., 109, E01012
Hardin, A. H., & Harvey, K. B. 1973, Spectrochim. Acta, 29A, 1139
Heavens, O. S. 1991, Optical Properties of Thin Films (New York: Dover)
Hudgins, D., Sandford, S. A., Allamandola, L. J., & Tielens, A. G. G. M. 1993, ApJS, 86, 713
Jenniskens, P., Blake, D. F., & Kouchi, A. 1998, in Solar System Ices, ed. B. Schmitt, C. de Bergh, & M. Festou (Norwell, MA: Kluwer), 139
Mastrapa, R. M., Bernstein, M. P., Sandford, S. A., Roush, T. L., Cruikshank, D. P., & Ore, C. M. D. 2008, Icarus, 197, 307
Mukai, T., & Krätschmer, W. 1986, EM&P, 36, 145
Narten, A. H., Venkatesh, C. G., & Rice, S. A. 1976, J. Chem. Phys., 64, 1106
Ockman, N. 1958, Adv. Phys., 7, 199
Petrenko, V. F., & Whitworth, R. W. 1999, Physics of Ice (Oxford: Oxford Univ. Press)
Roush, T. L. 1994, Icarus, 108, 243
Schmitt, B., Quirico, E., Trotta, F., & Grundy, W. M. 1998, in Solar System Ices, ed. B. Schmitt, C. de Bergh, & M. Festou (Norwell, MA: Kluwer), 199
Toon, O. B., Tolbert, M. A., Koehler, B. G., Middlebrook, A. M., & Jordan, J. 1994, J. Geophys. Res., 99, 25631
Warren, S. G. 1984, Appl. Opt., 23, 1206
Warren, S. G., & Brandt, R. E. 2008, J. Geophys. Res., 113, D14220
Westley, M. S., Baratta, G. A., & Baragiola, R. A. 1998, J. Chem. Phys., 108, 3321
Whalley, E. 1977, Can. J. Chem., 55, 3429